NCRA • TIFR

National Centre for Radio Astrophysics

Internal Technical Report
NCRA–GMRT/uGMRT/February 2020

Tests for determination of relative offsets and frequency definition for upgraded GMRT beamformer data

Bhal Chandra Joshi

Revision	Date	Modification/ Change
Ver 1	February 2, 2020	Initial Version
Ver 2	April 4, 2020	Fixed freq definition
Ver 3	June 2, 2020	Added test post new GWB software release

Contents

1 Introduction

The recent upgrades to the Giant Meterwave Radio Telescope (**uGMRT : Gupta et al., 2017)** has significantly increased the frequency coverage of the instrument. This has enabled a wide range of pulsar studies with the new instrument, where the wider bandwidths allow both higher sensitivity as well as astronomical studies as a function of frequency, both within the band and across multiple bands (For example, see Krishnakumar et al., 2017; Joshi et al., 2018; Maan et al., 2019). These studies need both an accurate definition of frequencies as well as relative offsets between the time-series acquired using multiple bands. These in turn depend on the mode of the observatory back-end. As the timestamps and frequency labelling of the pulsar data cube varies with the back-end mode used, these needed to be determined for the GMRT wide-band backend (GWB). Astronomical tests to calibrate these were carried out, which are briefly described in this report. The modes of GWB are briefly reviewed in Section 2. The experiments are described in Section 3 followed by analysis and results in Sections 4 and 5. The conclusions of the tests are enumerated in Section 6.

2 Brief Description of GWB modes

The data from 30 antennas of the GMRT are processed in the new wide-band uGMRT Wide-band backend (GWB : Reddy et al., 2017). The downconverted radio frequency voltages from each antenna are digitized, compensated for fixed instrumental delays and converted into spectral data using N-point Fast Fourier Transform (FFT), where N ranges from 2048 to 32764. The GWB can digitize data for three different bandwidths - 100, 200 and 400 MHz. In its samplest form, it provides an N-channel digital filterbank. The channel frequencies are determined by the standard FFT algorithm, where the centre of DC channel corresponds to local oscillator frequency (LO) and the channel centre incrments by bandwidth per channel (bwpch), obtained by dividing the acquisition bandwidth (BW) by the number of channels used (NCH). This has been confirmed by engineering tests (Reddy, 2019). The GWB further carries out correlation for interferometer and also compensates for fractional sampling time instrumental delay determined using a point phase calibrator source in interferometer mode. The spectral voltage from each antenna can be squared and added to form the Incoherent beam (IA beam) or added in phase to form a Phased array beam (PA beam). The GWB provides 4 such beams. In addition, real time coherent dedispersion can be carried out in the GWB hardware to obtain a coherently dedispersed beam (CDB). The GWB allows a variety of sampling time (tsamp) to be configured limited in number of channels (NCH) by the data rate only. For details, see Reddy (2017).

The main aim of these tests was to determine correctly the frequency labeling and the relative offsets between the different modes of the GWB beam-former. The procedure used for these tests is outlined in the next section.

3 Brief Description of the Experiment

While the enginneering tests (Reddy, 2019) characterize the frequency labeling and relative time offsets between different GWB modes for the recorded data, these need to be interpreted correctly and consistently by the astronomical data processing software. This requires observations of suitable astronomical radio sources, which provides a time and frequency marker. The relative offsets can be as large as a few seconds, so a source which emits a time marker separated by $10-100$ s is needed. A source which provides a strong frequency dependence of its emission

Table 1 Observation setup used on different epochs

		Epoch		
MJD		**58832**	**58871**	**58991**
Date		**Dec 16, 2019**	**Jan 24, 2020**	**May 22, 2020**
Number of subarrays and bands used	:	2	2	3
Simultaneous observations with ORT	:	No	No	Yes
	:	1460	1460	1460
Radio Frequencies used				650
		500	500	500
				334.5
Acquisition bandwidth GWB	:	100	100	100
Number of channels used in PA	:	1024	1024	1024
Number of subbands used in CDB	:	1024	256	64
Sampling time used in PA (μs)	:	81.92	81.92	40.96
Sampling time used in CDB (μs)	:	81.92	20.48	5.12
Acquisition bandwidth ORT	:			16
Sampling time used at ORT (μs)	:			32

is required as a frequency marker. These characteristics are present in the pulsed emission from high dispersion measure pulsars with Giant pulses (GPs). PSR B0531+21 (J0534+2200) is a bright pulsar in the Crab nebula, which emits sporadic intense GPs (Hankins et al., 2003), typically spaced 3 to 4 minutes apart. Moreover, these GPs have been seem simultaneously from 300 to 1500 MHz (Sallmen et al., 1999; Karuppusamy et al., 2012). The relatively high dispersion measure (DM) of this pulsar allows a sensitive probe of frequency definition as the arrival time of GPs are a strong function of frequency due to dispersion in the ionised inter-stellar medium. Moreover, the DM of this pulsar varies with observation epochs. As the pulsar is regularly monitored [1](Lyne et al., 1993), the variations in DM are known for calibration purpose. Hence, we chose this pulsar for this experiment.

In addition, the brightest northern hemisphere pulsar, PSR B0329+54 (J0332+5434) was also observed becasuse (a) single pulses from this pulsar are easily observable at all bands at the uGMRT and (b) the single pulse intensity varies from pulse to pulse with the single pulse pattern providing a time marker.

The observations were carried out at three epochs in December 16, 2019, January 24, 2020 and May 22, 2020. At each epoch, the GMRT antennas were divided into two or three subarrays with each subarray at a different band. All four beams of GWB were used in these experiments to record data simultaneously, with two beams being used for CDB mode and the other two in PA mode. The data were acquired with 1024 channels across 100 MHz band with different sampling times at each epoch. In case of CDB mode, the number of final subbands was different for each epoch. The data were recorded with a time-stamp derived from the observatory time standard, which consists of Global Positioning System (GPS). Simultaneous data was recorded using the Ooty Radio Telescope (ORT) on May 22, 2020. The details of the observations are given in Table 1.

[1]http://www.jb.man.ac.uk/pulsar/crab.html

Table 2 Timing and DM parameters of the pulsars used. Parameters for PSR J0534+2200 marked with ‡ were taken from Jodrell Bank Crab ephemeris Lyne et al. (1993)

Parameter		**PSR J0332+5434**	**PSR J0534+2200**
Right Ascension (J2000)	....	03h32m59.4096s	05h34m31.973s
Declination (J2000)	....	+54d34'43.329"	+22d00'52.06"
Proper Motion RA	....	16.97	-14.7
Proper Motion DEC	....	-10.37	2.0
Parallax	....	0.59	
Position Epoch	....	46473	40706
Frequency (F0)	....	1.399541538720	‡
F1	....	-4.011970E-15	‡
F2	....	5.3E-28	‡
Period Epoch	....	46473	‡
DM	....	26.7641	‡
DM Epoch	....	26.7641	‡

4 Data Analysis

The raw data for each beam (4 data sets on MJD 58832 and 58871 and 5 data sets on MJD 58991 were reduced to dedispersed time series after identifying narrow-band radio frequency interference (RFI) channels using outliers in root-mean-square variation in each channel. The time-series were folded using the pulsar ephemeris to single pulses. The dedispersion and folding were carried out using tools in SIGPROC package[2]. The pulsar parameters used for dedispersion and folding are given in Table 2. A constant DM was assumed for PSR J0332+5434, with pulsar ephemeris taken from the ATNF pulsar catalogue [3](Manchester et al., 2005). In case of PSR J0534+2200, DM and pulsar parameters, given in Jodrell Bank Crab ephemeris(Lyne et al., 1993), were used choosing the nearest available epoch of measurements for MJD 58832 and 58871, whereas DM was estimated from our own data for MJD 58991.

The GPs were identified from the single pulse data and dedispersed time-series of duration 5 s around the identified GP was extracted for each beam (band). These extracted time-series for two beams (bands) were then visually examined to check for the presence of the GP in each beam. The data around each GP were cross-correlated using a python script developed by us. The peak of the cross correlation provides the offset in the time-of-arrival of GP in each beam. This observed offset ($\delta\tau_{obs}$) was then compared with the expected offset ($\delta\tau_{exp}$), which takes into account the expected time delay due to dispersion in ionised inter-stellar medium, given by Equation 1, and any relative offset in the mode of observations (PA/IA/CDB/ORT).

$$\delta\tau_{dm} = 4148.808((1.0/\nu_1^2) - (1.0/\nu_2^2)) * DM \quad (1)$$

[2]http://sigproc.sourceforge.net/

[3]https://www.atnf.csiro.au/people/pulsar/psrcat/

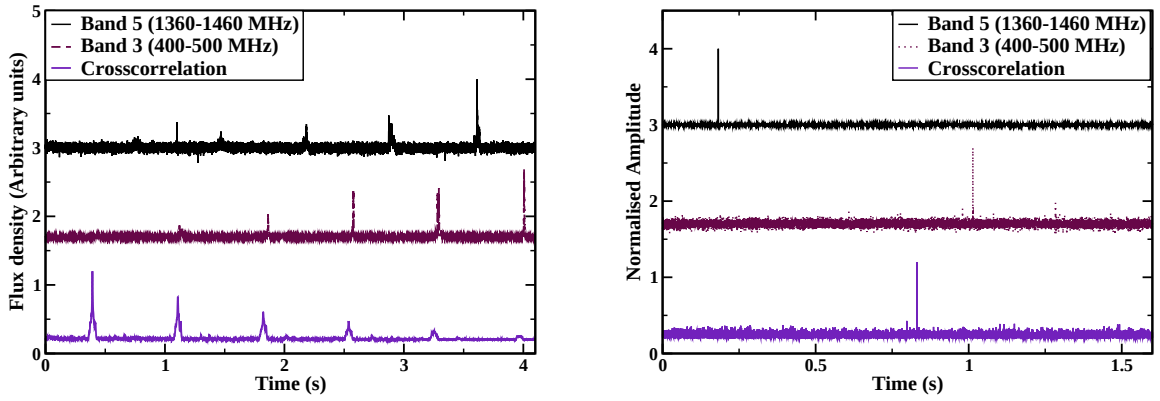

(a) PSR J0332+5434

(b) PSR J0534+2200

Figure 1 Time series observed using Band 5 (1360 – 1460 MHz : top plot in each panel) and Band 3 (400 – 500 MHz : middle plot in each panel) was used to determine the delay between the two bands using pulsars PSRs J0332+5434 and J0534+2200. The delay is obtained from the lag measured using the cross-correlation (shown in the bottom plot of each panel) of the two time series. The delay in each case was compared with that expected due to dispersion in ionised inter-stellar medium to determine both the frequency definition as well as relative pipeline delays : (a) Observations of single pulses of the bright pulsar J0332+5434 showing a delayed single pulse pattern in Band 3 compared to Band 4, (b) Observations of a Giant pulse of PSR J0534+2200 where the delay between Band 5 (top plot) and Band 3 (middle plot) was found consistent with that expected due to dispersion, assuming the correct frequency definitions (Equations 3a & 3b) and zero relative fixed pipeline delay.

Here, DM is the assumed dispersion measure of the pulsar and ν_1 and ν_2 are the radio frequencies to which the data was assumed to be dedispersed. It may be noted from Equation 1 that $\delta\tau_{dm}$ is very sensitive to assumed frequency definition, particularly at frequencies below 600 MHz and also varies with DM. The predicted $\delta\tau_{dm}$ will therefore vary with assumed radio frequencies and DM. Thus, consistency with the observed ($\delta\tau_{obs}$) can constrain the frequency definition with high precision, particularly over the three different epochs of this experiment, where the DM of PSR J0534+2200 varied by about 0.03 $\mathrm{pc\,cm^{-3}}$. The relative delays between the GWB modes (and ORT data acquisition system) are fixed on the other hand unless modified in the software. For MJD 58832 and 58871, a fixed relative pipeline delay was expected from engineering tests (Reddy, 2019), which was verified in the manner mentioned above. These delays were adjusted in March 2020 (Reddy, private communications) and the adjustment were again verified on MJD 58991.

Each data set was analysed using five different assumed frequency definitions. These are as follows

1. The zeroth channel assumed to be the local oscillator (LO) frequency (for example, 500.0 and 1460.0 MHz) for all modes
2. The zeroth channel assumed to be one channel below the LO frequency (for example, 1459.90234375 and 499.90234375 MHz) for all modes

3. The zeroth channel assumed to be half channel below the LO frequency (for example, 1459.951171875 and 499.951171875 MHz) for all modes

4. The zeroth channel assumed to be LO frequency for IA/PA modes and one below LO frequency for CDB mode (for example, 1459.90234375 and 500.0 MHz)

5. The zeroth channel assumed to be LO frequency for IA/PA modes and half a channel below LO frequency for CDB mode (for example, 1459.951171875 and 500.0 MHz)

Representative results of this analysis for PSR J0332+5434 and J0534+2200 are presented in Figure 1. These analysis were carried out for each of the three epochs for all four beams. The delay between different bands and beam modes were then measured ' for each case and compared with the expected delay as per the engineering interpretation and tests. The definition which most closely reproduces the measured delay is adopted as valid definition in the conclusions. As a side-product relative pipeline delay between the modes were also estimated.

5 Results

The results of these tests are presented in this section. The default GWB operations software was used on December 16, 2019 (MJD 58832) with two CDB mode beams, one each at Band 3 and Band 5 and two PA beams, one each at Band 3 and Band 5. A short stretch was also taken with IA beam. The offsets determined from the GPs on this epoch are presented in the Appendix (Figures $2 - 4$) for comparison between different pairs of GWB modes used. The delay between each pair is compared with that expected in Table 3. The fixed relative pipeline delay (Δ_{PQ}) is also indicated in the table. These results showed that there is a fixed relative pipeline delay between IA/PA modes and CDB mode of GWB. The delay is equal to time required for the number of samples in a 32 MByte buffer, which is given by Equation 2.

$$\Delta_{PQ} = tsamp \times 33554432/(2 \times nch) \tag{2}$$

Here, nch is the number of channels used and $tsamp$ is the sampling time.

Similar measurements were obtained from the GPs observed on January 24, 2020 (MJD 58871) and these are presented in the Appendix (Figures $5 - 7$) for comparison between different pairs of GWB modes used. A smaller number of channels and finer sampling resolution was used in this epoch for the CDB mode to verify the frequency and relative pipeline delay estimates. The results are tabulated in Table 3 and were consistent with those obtained in the previous epoch as well as expected from engineering definitions and tests.

Epoch (MJD)	DM (pc cm^{-3})	Band and Mode	Sampling Time (μs)	Expected delay (s)	Observed delay (s)	Δ_{PQ} s
58832	56.7528	B5CDB-B3CDB	81.92	0.83172	0.83165(8)	0.0
		B3CDB-B5PA	81.92	0.83173	0.83173(8)	1.34218
		B5CDB-B5PA	81.92	0.00001	0.00008(8)	1.34226
		B5PA-B3PA	81.92	0.83137	0.83141(8)	0.0
58871	56.7401	B5CDB-B3CDB	20.48	0.83259	0.83259(2)	0.0
		B3CDB-B5PA	81.92	2.1748	2.1746(2)	1.342177
		B5PA-B3PA	81.92	0.8312	0.8312(1)	0.0
58991	56.7781	B5CDB-B3CDB	5.12	0.8374	0.8375(1)	0.0
		B5CDB-B4PA	40.96	0.39062	0.39051(8)	0.0
		B3CDB-B4PA	40.96	0.4468	0.4470(2)	0.0
		B4PA-B5PA	40.96	0.4470	0.4472(2)	0.0
		B5PA-B5IA	40.96	0.0	0.0	0.0

Table 3 Results of time delay measurements simultaneously at two different frequency using PSR J0534+2200 for validating frequency definitions and relative pipeline delays (Δ_{PQ}) for different modes of pulsar observations. The epoch of observations is given in the first column along-with Dispersion measure at that epoch in second column followed by sampling time used, expected and observed delay in samples for different combination of modes at the two frequencies in fourth, fifth, sixth, seventh and third column respectively. The last column presents the relative pipeline delays (Δ_{PQ}). The abbreviations B5CDB, B3CDB, B5PA and B3PA indicate data acquisition using Band 5 in CDB mode, using Band 3 in CDB mode, Band 5 in PA mode, and Band 3 in PA mode respectively.

Based on the repeatability of results from these two epoch, the engineering team carried out suitable changes in the observatory software. This new version of software was again tested using enginnering tests, which involved using well defined frequency tones as well as a minute pulse time marker, obtained using GPS, being fed at the input. These tests indicated that there is no longer a relative pipeline delay between IA/PA and CDB modes. The new version was adopted for astronomical observations in March 2020. Astronomical tests to validate these were carried out on May 22, 2020 (MJD 58991) and the results of these tests are presented in the Appendix (Figures 5 − 7) for comparison between different pairs of GWB modes used. In this epoch, apart from using a much smaller number of channels and finer sampling resolution for CDB mode (than the past epoch MJD 58871), simultaneous observations with the ORT were also carried out, giving a larger variety of frequencies. The results are tabulated in Table 3 and were consistent with those obtained in the previous epoch as well as expected from engineering definitions and tests.

6 Summary and Conclusions

The frequency labeling for the different modes, expressed in terms of the value of the highest frequency channel (F_1), are given in the following expressions:
For IA and PA,

$$F_1 = \begin{cases} F_{\rm LO} & \text{for LSB} \\ F_{\rm LO} + \Delta F & \text{for USB} \end{cases}, \tag{3a}$$

and for CDB,

$$F_1 = \begin{cases} F_{\rm LO} - \frac{\Delta F}{N_{\rm chan}} & \text{for LSB} \\ F_{\rm LO} + \Delta F \left(1 - \frac{1}{N_{\rm chan}}\right) & \text{for USB} \end{cases}. \tag{3b}$$

Here, $F_{\rm LO}$ refers to the Local Oscillator (LO) frequency (MHz) used for the observations, ΔF is the acquisition bandwidth (typically 100 or 200 MHz) and $N_{\rm chan}$ denotes the number of

channels or sub-bands across the band. The expression is different for each side-band denoted by USB or LSB. When $F_{\rm LO}$ is chosen at the lowest edge of the band being used, this is called upper side-band (USB) where frequencies are ordered from lowest to highest frequency. The reverse order of frequencies are used in lower side-band (LSB) with the $F_{\rm LO}$ chosen at the highest edge of the band. Equations 3a-3b are in agreement with what is expected from the implementation of the IA, PA, and CDB pipelines in GWB (De & Gupta, 2016; Reddy et al., 2017).

References

De, K., & Gupta, Y. 2016, Experimental Astronomy, 41, 67

Gupta, Y., Ajithkumar, B., Kale, H., et al. 2017, Current Science, 113, 707

Hankins, T. H., Kern, J. S., Weatherall, J. C., & Eilek, J. A. 2003, nat, 422, 141

Joshi, B. C., Arumugasamy, P., Bagchi, M., et al. 2018, Journal of Astrophysics and Astronomy, 39, 51

Karuppusamy, R., Stappers, B. W., & Lee, K. J. 2012, aap, 538, A7

Krishnakumar, M. A., Joshi, B. C., & Manoharan, P. K. 2017, apj, 846, 104

Lyne, A. G., Pritchard, R. S., & Graham Smith, F. 1993, mnras, 265, 1003

Maan, Y., Joshi, B. C., Surnis, M. P., Bagchi, M., & Manoharan, P. K. 2019, apjl, 882, L9

Manchester, R. N., Hobbs, G. B., Teoh, A., & Hobbs, M. 2005, aj, 129, 1993

Reddy, S. H. 2017, OPERATING PROCEDURE FOR RUNNING GWB - IV

—. 2019, Timestamp flow in GWB and correction

Reddy, S. H., Kudale, S., Gokhale, U., et al. 2017, Journal of Astronomical Instrumentation, 06, 1641011

Sallmen, S., Backer, D. C., Hankins, T. H., Moffett, D., & Lundgren, S. 1999, apj, 517, 460

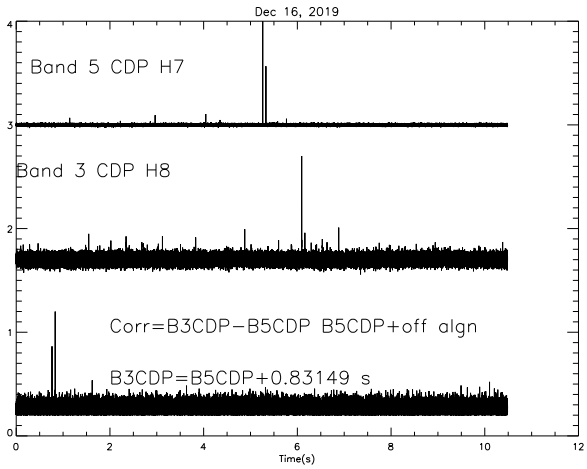

(a) B5 CDB and B3 CDB modes

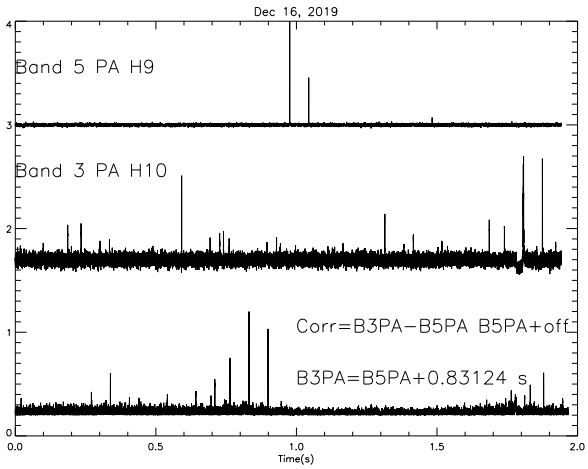

(b) B5 PA and B3 PA modes

Figure 2 Relative delays observed on December 16, 2019 (MJD 58832)

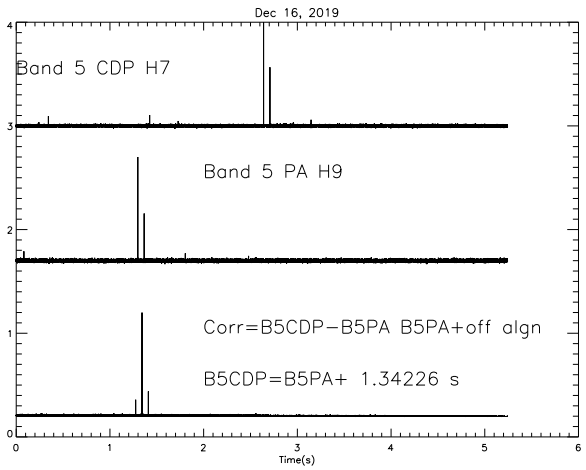

(a) B5 CDB and B5 PA modes

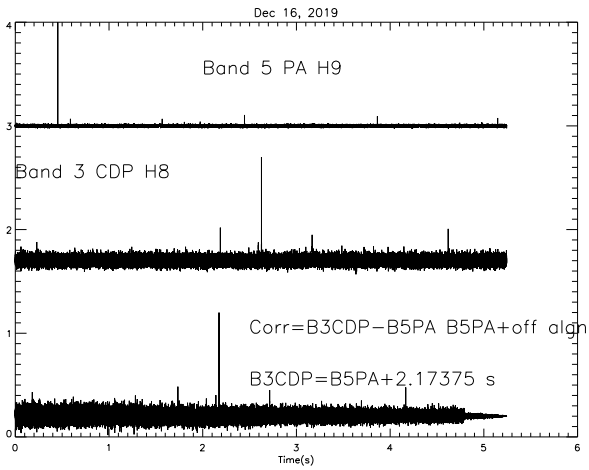

(b) B3 CDB and B5 PA modes

Figure 3 Relative delays observed on December 16, 2019 (MJD 58832)

Appendix A

The measurements of delay between different combinations of beams for the experiments on December 16, 2019, January 24 and May 22, 2020 are presented in this appendix.

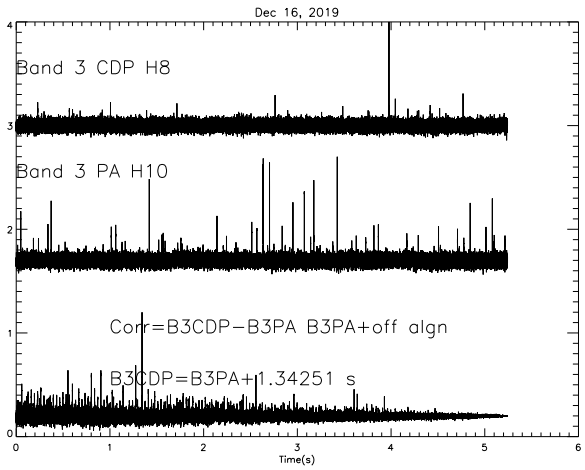

(a) B3 CDB and B3 PA modes

Figure 4 Relative delays observed on December 16, 2019 (MJD 58832)

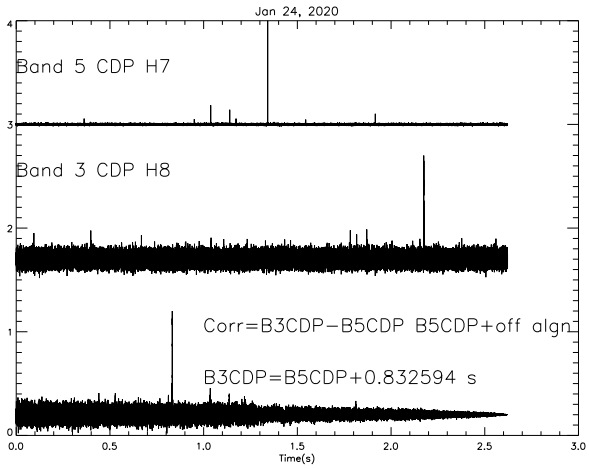

(a) B5 CDB and B3 PA modes

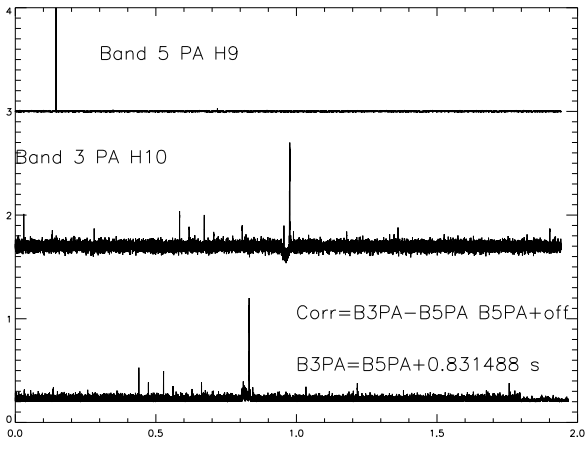

(b) B5 PA and B3 PA modes

Figure 5 Relative delays observed on January 24, 2020 (MJD 58871)

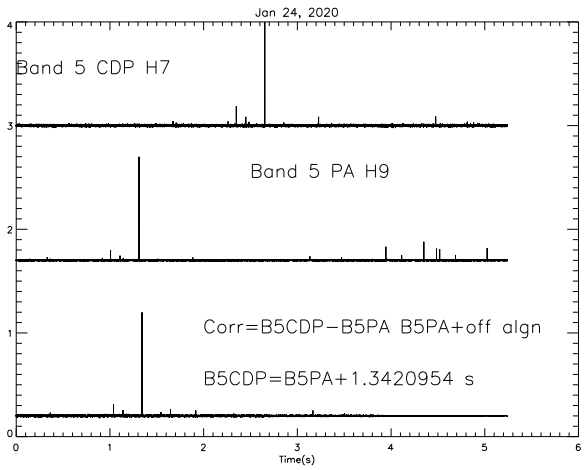

(a) B5 CDB and B5 PA modes

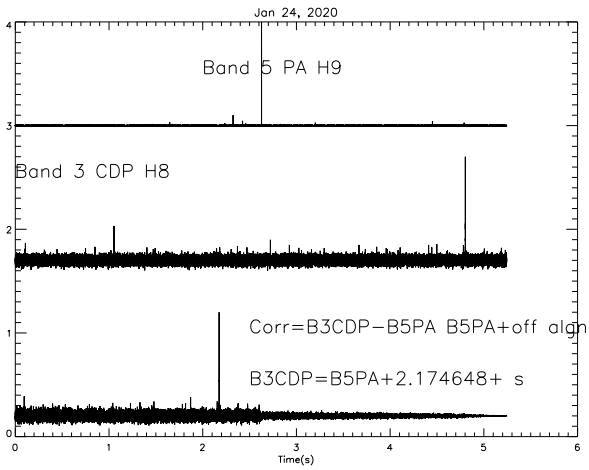

(b) B3 CDB and B5 PA modes

Figure 6 Relative delays observed on January 24, 2020 (MJD 58871)

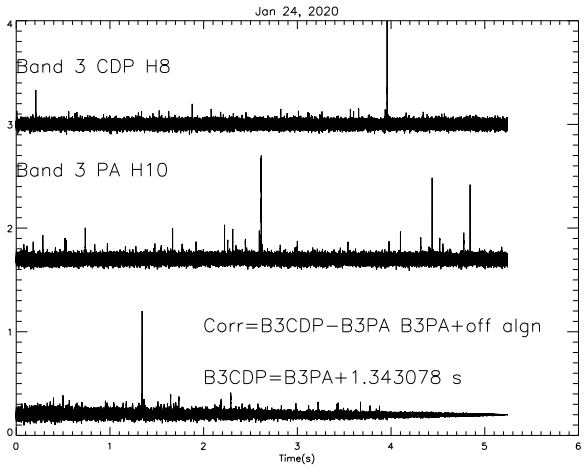

(a) B3 CDB and B3 PA modes

Figure 7 Relative delays observed on January 24, 2020 (MJD 58871)

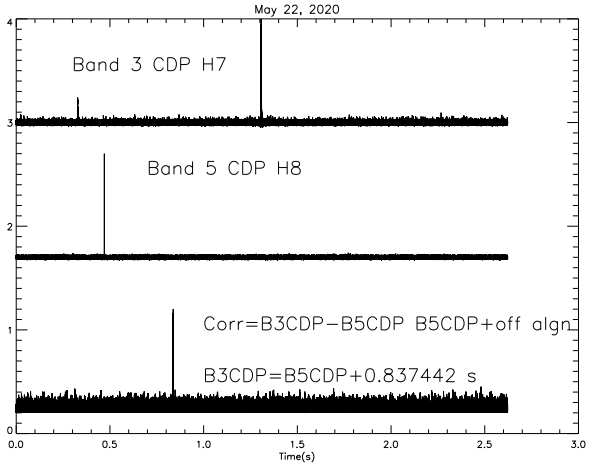

(a) PSR J0332+5434

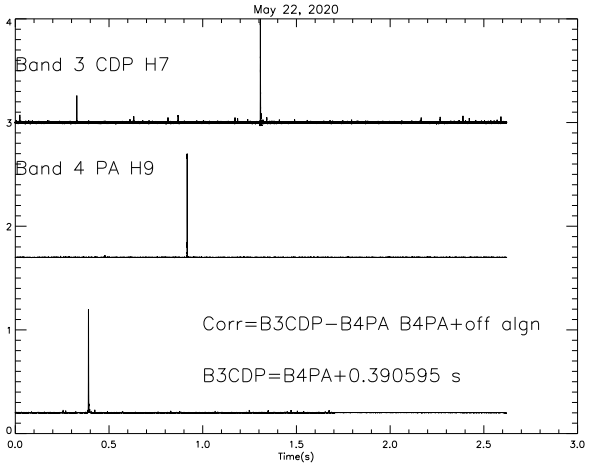

(b) PSR J0332+5434

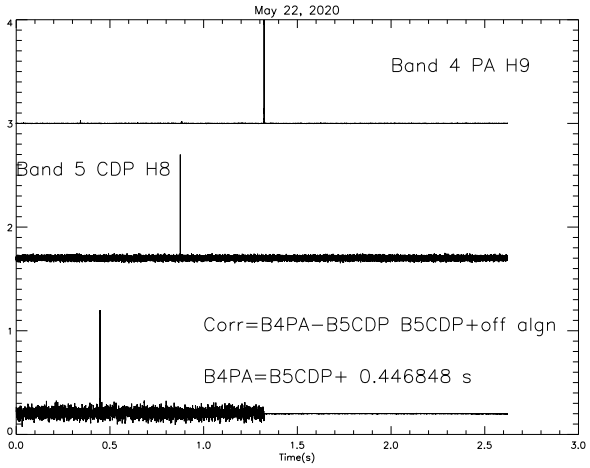

(a) PSR J0332+5434

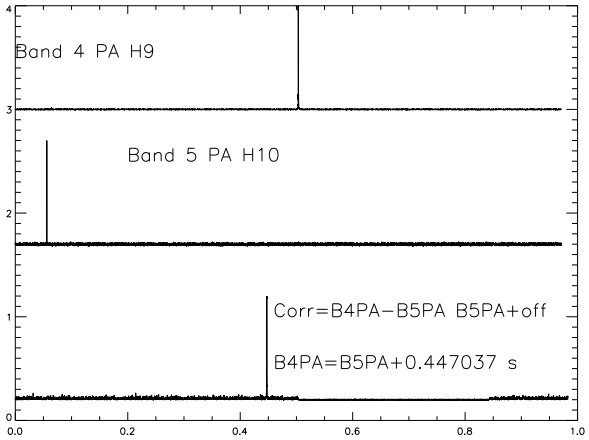

(b) PSR J0332+5434

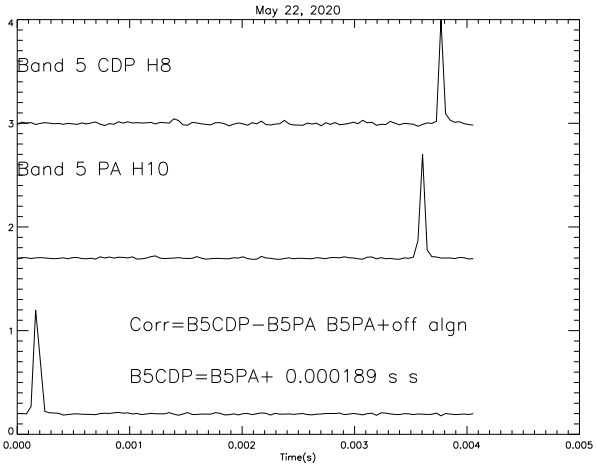

(a) PSR J0332+5434

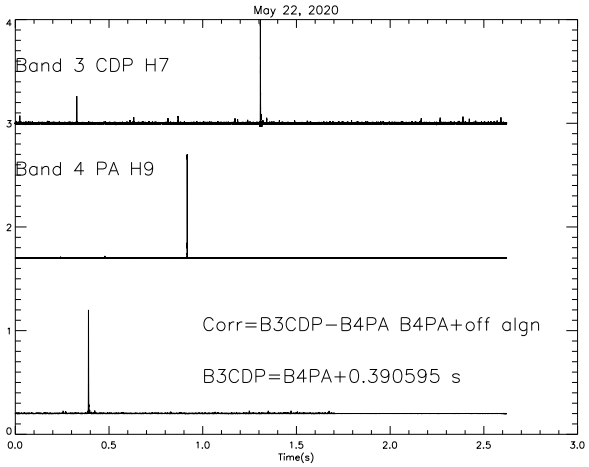

(b) PSR J0332+5434